Three-dimensional classical imaging of a pattern localized in a phase space

Mandip Singh* and Samridhi Gambhir
Department of Physical Sciences,
Indian Institute of Science Education and Research Mohali, Mohali 140306, India

(Received 4 April 2018; published 19 November 2018)

In most imaging experiments, the structure of an object is defined in a position space. Such a structural pattern can be stationary, or for a dynamic object it can be nonstationary with time. An image of such an optically responsive object can be produced with a lens, therefore such an object can be seen with a camera or by the human eye. In this paper, we go beyond the conventional notion of imaging. A structural pattern of objects in our experiment is defined in a phase space, therefore such a pattern cannot be imaged with a lens or a camera, and the human eye cannot visualize it. A pattern in phase space is produced from object transparencies and imprinted onto the phase space of an atomic gaseous medium of a Doppler-broadened absorption profile at room temperature by utilizing velocity-selective hole burning in the absorption profile. The pattern is localized in a unique three-dimensional phase space, which is a subspace of the six-dimensional phase space. Tomographic images of the localized phase-space pattern are captured at different momentum locations by a laser light that has never interacted with actual objects. In addition, imaging of an imprinted phase-space pattern of an object of nonuniform transmittance is presented.

DOI: 10.1103/PhysRevA.98.053828

Imaging of an absorptive and a transparent object located in a position space is usually produced from light reflected or transmitted by the object. A transparent object localized in a position space can be imaged with phase-contrast imaging methods in which variations of phase across a transparent object are converted to intensity variations [1–5]. Phase-contrast imaging is a nondestructive [6–9] technique to image a Bose-Einstein condensate [10–13]. In all such methods of imaging, light interacting with an object is detected to produce an image. In this paper, we go beyond imaging in position space and introduce three-dimensional (3D) tomographic imaging of a pattern that is localized in a phase space. In this imaging concept, light used to image the phase-space pattern never interacts with the actual position space objects. The pattern is localized in a unique 3D subspace of the six-dimensional (6D) phase space, involving two position coordinates and one momentum coordinate. However, the pattern is delocalized in a 3D position subspace and in a 3D momentum subspace of the 6D phase space separately. Experiments on imaging of objects localized only in the position space have been realized with quantum and classical methods with undetected photons [14,15] and ghost imaging [16–24]. In all such position space imaging experiments, a two-dimensional (2D) image is produced from photons that have never interacted with the object. The 3D tomographic imaging of a phase-space pattern presented in this paper can be utilized to store a pattern in phase space, and it can have practical applications to make a phase-space memory device.

In the experiment presented in this paper, the pattern of interest is produced from object transparencies and imprinted onto the phase space of an atomic gaseous medium at room temperature. The experiment is performed by utilizing velocity-selective hole burning [25–32] in a Doppler-broadened absorption profile of an atomic gaseous medium. Tomographic images of the pattern localized in a 3D phase space are then captured with an imaging laser beam. This laser beam does not interact with actual objects used to produce the localized phase-space pattern. A pattern of an object of nonuniform transmittance is also imprinted onto the phase space of an atomic medium, and the pattern is imaged at a constant location of momentum.

I. CONCEPT

A localized pattern in a 3D subspace of the 6D phase space is shown in Fig. 1(a), where a two dimensional position space is spanned by orthogonal position unit vectors $\hat{x}$ and $\hat{y}$ and a third dimension corresponds to the z component of momentum, p_z. In experiment, p_z is the z component of momentum of atoms. The pattern is stationary with time. A 2D planar section of a localized 3D phase space pattern at a constant p_z represents a tomogram of the localized pattern. In Fig. 1(a), three different tomograms at three different momenta are shown. Tomograms with an image of the English script letters **C**, **A**, and **T** are localized at p_z equals to p_1, p_2, and p_3, respectively. Furthermore, in a 3D position space, spanned by orthogonal position unit vectors $\hat{x}$, $\hat{y}$ and $\hat{z}$, each tomogram is completely delocalized on z-axis that implies, all images are overlapped with each other and distributed at all points on z-axis. However, in a 3D momentum space, spanned by orthogonal unit vectors $\hat{p}_x$, $\hat{p}_y$ and $\hat{p}_z$ of momentum components along $\hat{x}$, $\hat{y}$, and $\hat{z}$ directions, each tomogram is delocalized in all planes parallel to the p_x-p_y plane. A subspace where the pattern is completely localized is a unique 3D subspace of the 6D phase space, as shown in Fig. 1(a).

*mandip@iisermohali.ac.in

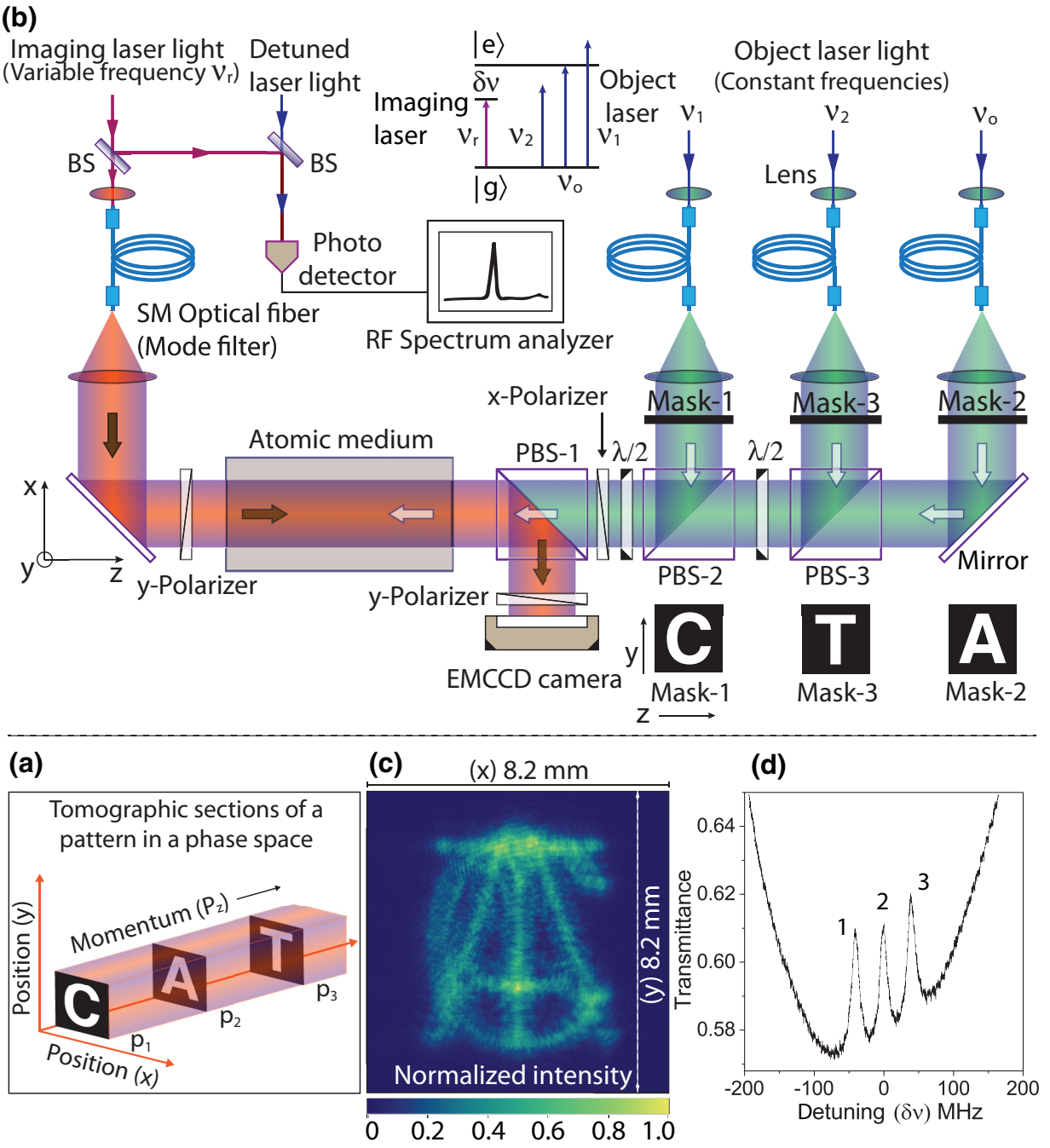

FIG. 1. (a) A pattern localized in a 3D phase space and its three tomograms. (b) Experimental schematic diagram; a linearly polarized imaging laser beam is overlapped in an atomic gaseous medium with counterpropagating object laser beams. A 2D transverse intensity profile of the imaging laser beam at different detunings is captured with an EMCCD camera. (c) A 2D transverse intensity profile of the overlapped object laser beams prior to their entrance into the atomic medium. All three letters are overlapped with each other. (d) Transmittance, for the imaging laser beam, of the atomic medium in the presence of object laser beams without masks. Three peaks labeled 1, 2, and 3 correspond to a velocity-selective hole-burning in a Doppler-broadened absorption profile produced by object laser beams of frequencies ν_1, ν_o, and ν_2, respectively.

In remaining 3D subspaces of the 6D phase space the pattern is delocalized. In this paper, a stationary localized 3D phase space pattern of interest is produced from objects located in the position space. The pattern is then imprinted onto the phase space of an atomic gas obeying Maxwell velocity distribution, in form of difference of number density of atoms in ground state and excited state. Tomographic images of the 3D phase space pattern are then imaged with an imaging laser beam, where by varying the frequency of the laser beam the location, p_z, of the tomogram can be shifted.

II. EXPERIMENTAL REALIZATION

A. Imprinting of a pattern onto a 3D phase space

A stationary pattern in the phase space of atoms is produced at room temperature (25 °C) by velocity-selective hole-burning in the Doppler-broadened absorption profile of an atomic gaseous medium. To understand how a pattern in phase space is produced, consider a linearly polarized object laser beam, of frequency ν_p and transverse intensity profile $I_p(x, y, \nu_p)$, propagating in an atomic gaseous medium in a direction opposite to the z axis. The intensity profile $I_p(x, y, \nu_p)$ represents a 2D image of an object in position space. This image information is transferred to a velocity class of the atomic gaseous medium at temperature T by velocity-selective atomic excitation. Consider an atomic gaseous medium where an isolated stationary atom has a ground quantum state $|g\rangle$ of energy E_g and an excited quantum state $|e\rangle$ of energy E_e with linewidth Γ. The object laser beam is on resonance with a velocity class of atoms of the z component of their velocity equals to $v_r = 2\pi(\nu_o - \nu_p)/k$, where $\nu_o = (E_e - E_g)/h$, $k = 2\pi/\lambda$ is the magnitude of the propagation vector of the object laser beam having wavelength λ. Atoms of other velocity classes are out of resonance due to the Doppler shift. The transverse Doppler shift is negligible because of the nonrelativistic velocity regime at room temperature. In the absence of an object laser beam, all the atoms are in the ground state. Consider n as the number of atoms per unit volume of the gaseous medium. According to Maxwell velocity distribution, a fraction of atoms with velocity in an interval dv_z around v_z at temperature T is $f(v_z)dv_z = (m/2\pi k_B T)^{1/2} e^{-mv_z^2/2k_B T} dv_z$, where k_B is the Boltzmann constant and m is the mass of an atom. Consider L as the length of the atomic medium along the beam-propagation direction. In the presence of an object laser beam, the ground-state atoms of resonant velocity class are populated to the excited state. A steady-state difference of atomic number densities in the ground state (n_1) and in the excited state (n_2) at v_z is $n_1(x, y, v_z) - n_2(x, y, v_z) = nf(v_z)/(1 + I_p(x, y, \nu_p)\Gamma^2/\{4I_s[(2\pi\nu_p - 2\pi\nu_o + kv_z)^2 + \Gamma^2/4]\})$, where I_s is the saturation intensity of the atomic transition. If attenuation and diffraction of the object laser beam are negligible, then the transverse intensity profile of the object laser beam is imprinted in the form of an atomic population difference in the resonating velocity class of atoms. This pattern is delocalized in the longitudinal direction, i.e., in the direction of propagation of the object laser beam, because atoms are uniformly distributed in the position space. However, the pattern is localized in the transverse plane of coordinates x, y at a z component of momentum of atoms, $p_z = mv_r$. If three different overlapping object laser beams of the same linear polarization but different intensity profiles and frequencies are passed through the atomic medium, then each beam imprints a different pattern in a different velocity class, where each one is located at a different p_z corresponding to the resonant velocity class of atoms addressed by the resonating object laser beam. As a result, a localized patten of all objects is imprinted onto a 3D subspace of the 6D phase space of atoms. The nearest frequency separation of object laser beams has to be much larger than the linewidth of the transition to reduce the overlapping of resonating velocity classes.

To image the localized phase-space pattern, a counterpropagating linearly polarized imaging laser beam of frequency ν_r is overlapped with the object laser beams passing through the atomic gaseous medium. The polarization of the imaging laser beam is perpendicular to the polarization of the object laser beams. The total absorption coefficient α of the imaging laser beam at frequency detuning, $\delta\nu = \nu_r - \nu_o$, is a convolution of population difference and absorption cross section of an atom such that $\alpha(x, y, \delta\nu) = \int_{-\infty}^{\infty}[n_1(x, y, v_z) - n_2(x, y, v_z)]\sigma_o(\Gamma^2/4)dv_z/[(2\pi\delta\nu - kv_z)^2 + \Gamma^2/4]$, where σ_o is the peak absorption cross section of the atomic transition. The absorption of the imaging laser beam decreases if it interacts with a velocity class of atoms excited by object laser beams, i.e., $n_2(x, y, v_z)$ is nonzero. This produces velocity-selective hole-burning in the Doppler-broadened absorption profile of the atomic medium. For the incident transverse intensity profile of the imaging laser beam $I_r(x, y, \delta\nu)$, the transmitted imaging laser beam intensity profile after passing through the gaseous medium is $I_r(x, y, \delta\nu)\exp(-\mathrm{OD}(x, y, \delta\nu))$, where $\mathrm{OD}(x, y, \delta\nu) = \alpha(x, y, \delta\nu)L$ is the optical density of the atomic medium. The optical density profile, at a detuning $\delta\nu$, corresponds to a tomographic section of the phase-space pattern at $p_z = 2\pi m\delta\nu/k$. The optical density, for the imaging beam at some frequencies, decreases if object laser beams are present. An image of a tomographic section can be constructed by measuring a change in the optical density profile caused by object laser beams. A 3D image of the phase-space pattern can be constructed with tomograms obtained at different detunings of the imaging laser beam.

In experiment, objects are three 2D transparency masks, where each mask consists of an image of a letter, **C** (on mask-1), **A** (on mask-2), and **T** (on mask-3), as shown in Fig. 1(b). All letters are transparent, and the remaining part of each mask is completely opaque to light. Object laser beams are initially passed through single-mode (SM) polarization maintaining optical fibers to produce beams of a Gaussian transverse intensity profile, where optical fibers are utilized as transverse mode filters. The mode-filtered and -collimated object laser beams of frequencies ν_1, ν_o, and ν_2 are then passed through mask-1, mask-2, and mask-3, respectively. After the masks, the transverse intensity profile of object laser beams corresponds to **C** (at ν_1), **A** (at ν_o), and **T** (at ν_2). All three object laser beams are overlapped on polarization beamsplitters (PBS-3, PBS-2). The overlapped object laser beams are linearly x-polarized by a polarizer with its pass axis aligned along the x axis (x polarizer). Two half-wave-plates are placed, before and after the PBS-2, to rotate the linear polarization of the object laser beams to equalize the intensity. The image of the transverse intensity profile of the overlapped object laser beams, prior to their entrance into the atomic medium, is shown in Fig. 1(c), where images of letters overlap with each other. A different letter is imprinted on a light field of different frequency and momentum. Therefore, an intensity profile of each object laser beam also corresponds to a tomograph in the 3D phase space.

B. Experimental method

The overlapped object laser beams are passed through an atomic gaseous medium, which is a 10-cm-long rubidium (^{87}Rb) vapor cell shielded from an external magnetic field. The linewidth of the resonant transition of the atomic medium is broadened due to the Doppler shift caused by the motion of atoms. An object laser beam of frequency ν_o is on resonance to the atomic transition of stationary ^{87}Rb atoms where a ground quantum state is $5\,^2S_{1/2}$ with a total angular momentum quantum number $F = 2$ ($|g\rangle$), and an excited quantum state is $5\,^2P_{3/2}$ with $F = 3$ ($|e\rangle$). For stationary atoms, the wavelength of this transition is $\lambda \simeq 780$ nm. Object and imaging beams are independently produced by single-mode and tunable extended cavity diode lasers. Object laser frequency is stabilized to the atomic transition, and three object beams of different frequencies are produced by shifting object laser light frequency with acousto-optic modulators. The frequency-shifted light is passed through SM polarization maintaining optical fibers to produce Gaussian beams. Object laser frequency ν_2 is red detuned by -40 MHz and frequency ν_1 is blue detuned by $+40$ MHz from the resonant transition for stationary atoms, as shown in Fig. 1(b). The nearest frequency separation of object laser beams is much larger than the linewidth, 5.75 MHz, and much lower than the Doppler broadening of the resonant transition. The frequency spread of all laser beams is less than 1 MHz. Frequency detuning of beams is measured with a resolution 0.1 MHz.

An object laser beam of frequency ν_o is on resonance with an atomic velocity class of $v_z = 0$. Therefore, an image of a letter **A** is imprinted in the zeroth velocity class in the form of an atomic population difference. An object laser beam of frequency ν_1 is on resonance with a velocity class $v_z = -31.2$ m/s, therefore an image of a letter **C** is imprinted in this velocity class of atoms. An object laser beam of frequency ν_2 is on resonance with a velocity class $v_z = +31.2$ m/s, therefore an image of a letter **T** is imprinted in this velocity class of atoms. Atoms of each velocity class are uniformly distributed in the position space volume of the atomic gaseous medium. Therefore, the imprinted pattern is completely delocalized along the length of the atomic gaseous medium in the beam propagation direction. All the imprinted images form a localized pattern in a unique 3D subspace of the 6D phase space of the atomic gaseous medium.

III. TOMOGRAPHIC IMAGING OF A 3D PHASE-SPACE PATTERN

To image the imprinted phase-space pattern, a linearly polarized imaging laser beam is passed through the atomic medium in the opposite direction relative to the propagation direction of object laser beams. Object and imaging laser beams are produced by two independent lasers. The imaging laser is also frequency-locked to the same resonant transition of stationary atoms, and its frequency is shifted by acousto-optic modulators. Prior to their entrance into the atomic medium, the transverse intensity profile of an imaging laser beam of frequency ν_r and detuning $\delta\nu = \nu_r - \nu_o$ is $I_r(x, y, \delta\nu)$. The imaging laser beam is y-polarized, which is perpendicular to the linear polarization of object laser beams, and its peak intensity is much lower than the saturation intensity of the atomic transition. After passing through the atomic medium, the imaging laser beam is reflected by PBS-1 and its transverse intensity distribution at different detunings is captured with an electron-multiplying charge-coupled-device (EMCCD) camera without gain multiplication. Transmittance of the atomic vapor cell for the imaging laser beam, at different detuning $\delta\nu$, in the presence of object laser beams without masks is shown in Fig. 1(d). Three peaks labeled 1, 2, and 3 correspond to velocity-selective hole-burning in a Doppler-broadened absorption profile caused by object laser beams of frequencies ν_1, ν_o, and ν_2, respectively. Object and imaging laser beams are counterpropagating, therefore a peak in the transmittance due to a hole-burning by a higher-frequency object laser beam appears at lower frequency of the imaging laser beam. To measure the imaging laser beam detuning precisely, part of the object laser light is extracted and red detuned by 190 MHz from the resonant transition. The extracted object laser light is overlapped with a part of the imaging laser light of the same polarization on a nonpolarization beamsplitter (BS). A beating signal of two lasers is detected with a fast response photodetector and measured with a radiofrequency spectrum analyzer as shown in Fig. 1(b). Detuning is measured from the frequency of the beating signal, which corresponds to a frequency difference of two lasers.

The intensity profile of the imaging laser beam after traversing through the atomic medium in the presence of object laser beams is $I_{\rm on}(x, y, \delta\nu) = I_r(x, y, \delta\nu)\exp(-{\rm OD}(x, y, \delta\nu))$. The optical density ${\rm OD}(x, y, \delta\nu)$ is constructed at detuning $\delta\nu$. The optical density is higher in the absence of object laser beams. A change in the optical density after switching-on the object laser beams is $\Delta{\rm OD}(x, y, \delta\nu) = -\ln[I_{\rm on}(x, y, \delta\nu)/I_{\rm off}(x, y, \delta\nu)]$, where $I_{\rm off}(x, y, \delta\nu)$ is the intensity profile of the imaging laser beam after traversing through the atomic medium in the absence of object laser beams. The frequency of the imaging laser beam is red detuned by $\delta\nu = -40$ MHz from the resonant transition. Its transverse intensity profile $I_{\rm off}(x, y, \delta\nu)$ is captured with an EMCCD camera in the absence of three object laser beams. After a time delay, another image of the imaging laser beam intensity $I_{\rm on}(x, y, \delta\nu)$ is captured in the presence of three object laser beams. A y-polarizer is placed in front of the EMCCD camera to block any backreflection of object laser beams from optical components. A change in the optical density profile, $\Delta{\rm OD}(x, y, \delta\nu) = -\ln[I_{\rm on}(x, y, \delta\nu)/I_{\rm off}(x, y, \delta\nu)]$, of the atomic medium is evaluated. Similar measurements are performed for detuning $\delta\nu = 0$ and $= +40$ MHz. In this way, for each detuning of the imaging laser beam, a different tomographic section of the 3D phase space localized pattern is captured. A series of three tomographic images are shown in Fig. 2 for three different detunings. The imaging laser beam is reflected by PBS-1, therefore images are constructed after making a reflection transformation in a plane parallel to the y-z plane, and $\Delta{\rm OD}(x, y, \delta\nu)$ is transformed to $\Delta{\rm OD}(z, y, \delta\nu)$. Three tomographic images resemble the English letters of object transparencies, i.e., **C** (at $\delta\nu = -40$ MHz), **A** (at $\delta\nu = 0$ MHz), and **T** (at $\delta\nu = +40$ MHz). By combining all the tomographic images, the word

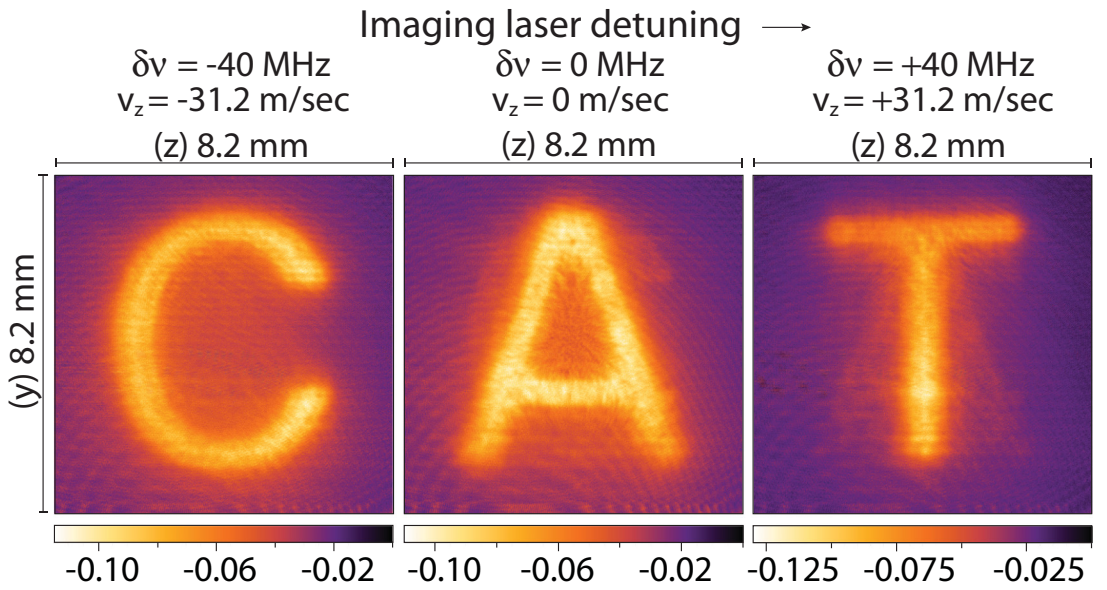

FIG. 2. Three tomographic images of a localized pattern in the 3D phase space captured at different detunings of the imaging laser beam. Each image is a plot of a change in the optical density, $\Delta\mathrm{OD}(z, y, \delta\nu)$.

CAT is formed, as shown in Fig. 2. Imaging laser beam detuning and the z component of the resonating velocity class corresponding to each tomographic image are shown on top of each tomograph.

In another experiment, an object of nonuniform transmittance is constructed by overlapping two neutral density filters of neutral densities (ND) 0.3 and 0.6 as shown in a photograph, Fig. 3(a). Four different regions R_1 (ND = 0), R_2 (ND = 0.3), R_3 (ND = 0.6), and R_4 (ND = 0.9) are formed. This object is positioned in place of a mask-2 in the path of an object laser beam of frequency ν_o. The image of a part of the object enclosed by a square as shown in Fig. 3(a) is captured with an imaging laser beam. The experiment is performed with a single object laser beam. The intensity profile $I_p(x, y, \delta\nu = 0)$ of the object laser beam after passing through the object consists of four different regions of different intensity levels. Therefore, it produces four regions of different depths of hole-burning in an atomic gaseous medium. The imaging laser beam is on resonance with velocity class $v_z = 0$, and an image of $\Delta\mathrm{OD}(z, y, \delta\nu = 0)$ of the atomic gaseous medium is constructed as shown in Fig. 3(b), which is an image of the overlapping neutral density filters.

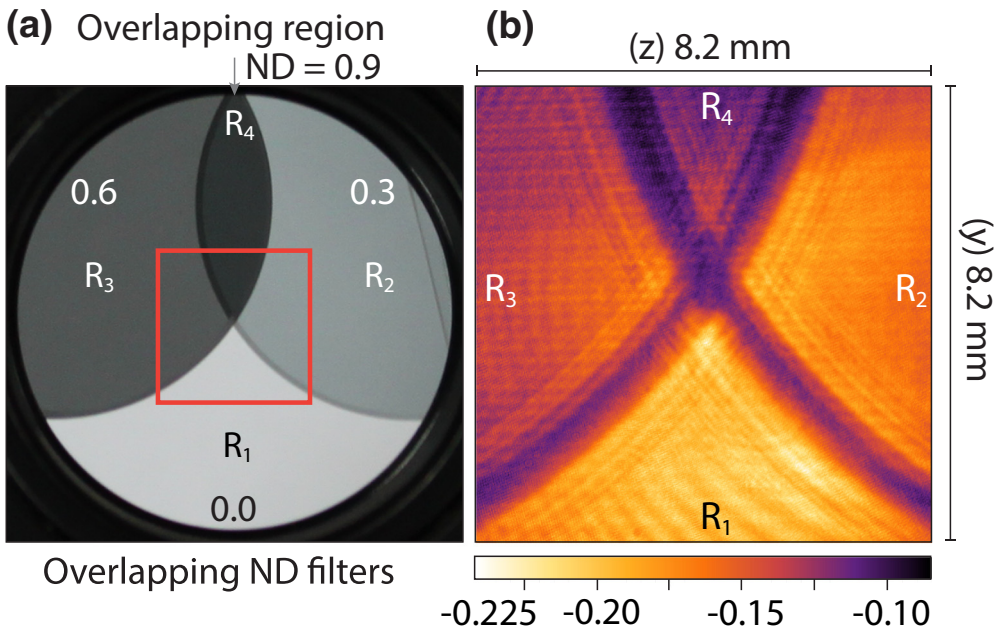

FIG. 3. (a) A photograph of overlapping neutral density filters. (b) An image, $\Delta\mathrm{OD}(z, y, \delta\nu = 0)$, of an area enclosed by a square as shown in (a).

IV. CONCLUSION

The experiment presented in this paper provides a way to produce a pattern localized in a unique 3D subspace of the 6D phase space. Tomographic imaging of the localized pattern is shown at three different locations of momentum. Therefore, a concept of producing and imaging a pattern in phase space is introduced, and its experimental implementation is clearly demonstrated in this paper. A phase-space pattern of a position space object of nonuniform transmittance is also produced and imaged at a constant location of momentum. This experiment can have a practical significance to produce a memory device in the phase space where information can be stored in a higher-dimensional phase space. The possibility of realizing such a phase-space memory device can be inspired by the concept and experiment presented in this paper.

[1] F. Zernike, Phase contrast, a new method for the microscopic observation of transparent objects, Physica **9**, 686 (1942).

[2] F. Zernike, Phase contrast, a new method for the microscopic observation of transparent objects, part ii, Physica **9**, 983 (1942).

[3] F. Zernike, How I discovered phase contrast, Science **121**, 345 (1955).

[4] S. W. Wilkins, T. E. Gureyev, D. Gao, A. Pogany, and A. W. Stevenson, Phase-contrast imaging using polychromatic hard X-rays, Nature (London) **384**, 335 (1996).

[5] T. J. Davis, D. Gao, T. E. Gureyev, A. W. Stevenson, and S. W. Wilkins, Phase-contrast imaging of weakly absorbing materials using hard X-rays, Nature (London) **373**, 595 (1995).

[6] M. R. Andrews, M.-O. Mewes, N. J. van Druten, D. S. Durfee, D. M. Kurn, and W. Ketterle, Nondestructive observation of a Bose condensate, Science **273**, 84 (1996).

[7] J. M. Higbie, L. E. Sadler, S. Inouye, A. P. Chikkatur, S. R. Leslie, K. L. Moore, V. Savalli, and D. M. Stamper-Kurn, Direct Nondestructive Imaging of Magnetization in a Spin-1 Bose-Einstein Gas, Phys. Rev. Lett. **95**, 050401 (2005).

[8] M. Kohnen, P. G. Petrov, R. A. Nyman, and E. A. Hinds, Minimally destructive detection of magnetically trapped atoms using frequency-synthesized light, New. J. Phys. **13**, 085006 (2011).

[9] M. Gajdacz, P. L. Pedersen, T. Morch, A. J. Hilliard, J. Arlt, and J. F. Sherson, Non-destructive Faraday imaging of dynamically controlled ultracold atoms, Rev. Sci. Instrum. **84**, 083105 (2013).

[10] K. B. Davis, M.-O. Mewes, M. R. Andrews, N. J. van Druten, D. S. Durfee, D. M. Kurn, and W. Ketterle, Bose-Einstein Condensation in a Gas of Sodium Atoms, Phys. Rev. Lett. **75**, 3969 (1995).

[11] M. H. Anderson, J. R. Ensher, M. R. Matthews, C. E. Wieman, and E. A. Cornell, Observation of Bose-Einstein condensation in a dilute atomic vapor, Science **269**, 198 (1995).

[12] P. Treutlein, D. Hunger, S. Camerer, T. W. Hänsch, and J. Reichel, Bose-Einstein Condensate Coupled to a Nanomechanical Resonator on an Atom Chip, Phys. Rev. Lett. **99**, 140403 (2007).

[13] W. Ketterle, D. S. Durfee, and Stamper D. M. Kurn, *Making, Probing and Understanding Bose-Einstein Condensates*, edited by M. Inguscio, S. Stringari, and C. E. Wieman, Bose-Einstein Condensation in Atomic Gases, Proceedings of the International School of Physics "Enrico Fermi," Course CXL (1999).

[14] G. B. Lemos, V. Borish, G. D. Cole, S. Ramelow, R. Lapkiewicz, and A. Zeilinger, Quantum imaging with undetected photons, Nature (London) **512**, 409 (2014).

[15] J. H. Shapiro, D. Venkatraman, and F. N. C. Wong, Classical imaging with undetected photons, Sci. Rep. **5**, 10329 (2015).

[16] T. B. Pittman, Y. H. Shih, D. V. Strekalov, and A. V. Sergienko, Optical imaging by means of two-photon quantum entanglement, Phys. Rev. A **52**, R3429 (1995).

[17] A. F. Abouraddy, P. R. Stone, A. V. Sergienko, B. E. A. Saleh, and M. C. Teich, Entangled-Photon Imaging of a Pure Phase Objects, Phys. Rev. Lett. **93**, 213903 (2004).

[18] A. Gatti, E. Brambilla, and L. Lugiato, Quantum imaging, Prog. Opt. **51**, 251 (2008).

[19] R. S. Aspden, D. S. Tasca, R. W. Boyd, and M. J. Padgett, EPR-based ghost imaging using a single-photon-sensitive camera, New. J. Phys. **15**, 073032 (2013).

[20] R. S. Bennink, S. J. Bentley, and R. W. Boyd, Two-Photon Coincidence Imaging with a Classical Source, Phys. Rev. Lett. **89**, 113601 (2002).

[21] A. Valencia, G. Scarcelli, M. D'Angelo, and Y. Shih, Two-Photon Imaging with Thermal Light, Phys. Rev. Lett. **94**, 063601 (2005).

[22] J. H. Shapiro, Computational ghost imaging, Phys. Rev. A **78**, 061802(R) (2008).

[23] F. Ferri, D. Magatti, A. Gatti, M. Bache, E. Brambilla, and L. A. Lugiato, High-Resolution Ghost Image and Ghost Diffraction Experiments with Thermal Light, Phys. Rev. Lett. **94**, 183602 (2005).

[24] M. Ghalaii, M. Afsary, S. Alipour, and A. T. Rezakhani, Quantum imaging as an ancilla-assisted process tomography, Phys. Rev. A. **94**, 042102 (2016).

[25] W. E. Lamb, Jr., Theory of an optical maser, Phys. Rev. **134**, A1429 (1964).

[26] W. R. Bennett, Jr., Hole burning effects in a He-Ne optical maser, Phys. Rev. **126**, 580 (1962).

[27] S. Haroche and F. Hartmann, Theory of saturated-absorption line shapes, Phys. Rev. A **6**, 1280 (1972).

[28] P. Siddons, C. S. Adams, C. Ge, and I. G. Hughes, Absolute absorption on rubidium d lines: comparison between theory and experiment, J. Phys. B **41**, 155004 (2008).

[29] M. L. Harris, C. S. Adams, S. L. Cornish, I. C. McLeod, E. Tarleton, and I. G. Hughes, Polarization spectroscopy in rubidium and cesium, Phys. Rev. A **73**, 062509 (2006).

[30] L. P. Maguire, R. M. W. van Bijnen, E. Mese, and R. E. Scholten, Theoretical calculation of saturated absorption spectra for multi-level atoms, J. Phys. B **39**, 2709 (2006).

[31] M. A. Hafiz, D. Brazhnikov, G. Coget, A. Taichenachev, V. Yudin, E. de Clercq, and R. Boudot, High-contrast sub-Doppler absorption spikes in a hot atomic vapor cell exposed to a dual-frequency laser field, New. J. Phys. **19**, 073028 (2017).

[32] S. Putz, A. Angerer, D. O. Krimer, R. Glattauer, W. J. Munro, S. Rotter, J. Schmiedmayer, and J. Majer, Spectral hole burning and its application in microwave photonics, Nat. Photon. **11**, 36 (2017).